

# Covalent bond symmetry breaking and protein secondary structure

Martin Lundgren<sup>1,\*</sup> and Antti J. Niemi<sup>2,1,†</sup>

<sup>1</sup>*Department of Physics and Astronomy, Uppsala University, P.O. Box 803, S-75108, Uppsala, Sweden*  
<sup>2</sup>*Laboratoire de Mathématiques et Physique Théorique CNRS UMR 6083,  
 Fédération Denis Poisson, Université de Tours, Parc de Grandmont, F37200, Tours, France*

Both symmetry and organized breaking of symmetry have a pivotal rôle in our understanding of structure and pattern formation in physical systems, including the origin of mass in the Universe and the chiral structure of biological macromolecules. Here we report on a new symmetry breaking phenomenon that takes place in all biologically active proteins, thus this symmetry breaking relates to the inception of life. The unbroken symmetry determines the covalent bond geometry of a sp<sup>3</sup> hybridized carbon atom. It dictates the tetrahedral architecture of atoms around the central carbon of an amino acid. Here we show that in a biologically active protein this symmetry becomes broken. Moreover, we show that the pattern of symmetry breaking is in a direct correspondence with the local secondary structure of the folded protein.

Protein modeling is based on various well tested and broadly accepted stereochemical paradigms [1], [2]. These paradigms are instrumental in protein structure prediction [3], and underlie the phenomenological force fields that describe protein dynamics [4]. The enormous success in resolving over 70.000 structures that are presently in Protein Data Bank (PDB) [5] is a clear manifestation that the various paradigms are valid to a high precision. Among the important paradigms is the assumption that the backbone C<sub>α</sub> carbons are in a definite sp<sup>3</sup> hybridized state, with its distinct tetrahedral geometry. For example the backbone τ<sub>NC</sub> ≡ (N-C<sub>α</sub>-C) bond angle should always fluctuate around a definite and computable value that only depends on the covalent bonds between the C<sub>α</sub> and its adjacent C<sub>β</sub>, N, C and H atoms. In particular, this value should *not* depend on the secondary structure environment.

With the arrival of third-generation synchrotron X-ray sources and the ensuing rapid increase in the number of protein structures that are being resolved with an ultrahigh sub-Ångström resolution it is now possible to experimentally scrutinize the validity of these paradigms. In particular any systematic, secondary structure dependent *breaking* of the covalent tetrahedral symmetry around the C<sub>α</sub> carbons could help us to better understand why proteins fold and to predict more accurately how they fold. This could also have major repercussions to pharmaceutical drug development, and to help us better understand what is life.

A molecular dynamics force field explicitly assumes that the tetrahedral symmetry remains unbroken. But *ab initio* quantum mechanical calculations [6] and empirical studies [7]-[9] have already pointed out that tetrahedral bond angles around a sp<sup>3</sup> hybridized carbon may be subject to measurable fluctuations. For example, there is an estimate that the τ<sub>NC</sub> ≡ (N-C<sub>α</sub>-C) bond angle could fluctuate as much as 8.8° [7] around its equilibrium position. This would have clearly measurable effects on the way how proteins fold. But the potential existence of a systematic and secondary structure dependent tetrahedral symmetry breaking have until now not been scrutinized.

Here we address the presence of a systematic tetrahedral symmetry breaking by investigating the secondary structure dependence in the values of τ<sub>NC</sub>, and in the adjacent τ<sub>Nβ</sub> ≡ (N-C<sub>α</sub>-C<sub>β</sub>) and τ<sub>Cβ</sub> ≡ (C-C<sub>α</sub>-C<sub>β</sub>) bond angles. In order to diminish any bias towards paradigm based refinements we inspect several subsets in Protein Data Bank (PDB). These include the canonical one that comprises all PDB configurations with resolution 2.0 Å or better, and its subsets with resolution better than 1.5 Å, and better than 1.0 Å. We also inspect a subset of the 2.0 Å set that contains only those proteins that have less than 30% sequence similarity, and finally we also consider those proteins that appear in the CATH classification. We find that our conclusions are independent of the data set we use, and for illustrative purposes we use the canonical 2.0Å set.

The conventional backbone Ramachandran torsion angles φ, ψ and ω relate to the backbone atoms N and C that we investigate. To diminish potential bias that may depend on refinement procedures, we here adopt the N and C independent, geometrically determined backbone Frenet frames; we follow the construction described in [10]. These frames depend *only* on the positions of the C<sub>α</sub> carbon coordinates **r**<sub>*i*</sub> with *i* = 1, ..., *n* labeling the residues. We first introduce the unit backbone tangent (**t**) and binormal (**b**) vectors

$$\mathbf{t}_i = \frac{\mathbf{r}_{i+1} - \mathbf{r}_i}{|\mathbf{r}_{i+1} - \mathbf{r}_i|} \quad \& \quad \mathbf{b}_i = \frac{\mathbf{t}_{i-1} \times \mathbf{t}_i}{|\mathbf{t}_{i-1} \times \mathbf{t}_i|} \quad (1)$$

With the unit normal vector **n**<sub>*i*</sub> = **b**<sub>*i*</sub> × **t**<sub>*i*</sub> we have the full orthonormal Frenet frame at the location of each C<sub>α</sub>. The bond angles and torsion angles are

$$\kappa_i = \arccos(\mathbf{t}_{i+1} \cdot \mathbf{t}_i) \quad \& \quad \tau_i = \arccos(\mathbf{b}_{i+1} \cdot \mathbf{b}_i) \quad (2)$$

The Frenet framing describes the position of all atoms of the protein, in the way how these atoms are seen by an imaginary observer who roller-coasts the backbone along the  $C_\alpha$  atoms with gaze direction always fixed towards the next  $C_\alpha$  [10]. In Figure 1 we display the statistical angular distribution of the backbone N and C and the side-chain  $C_\beta$  atoms in our PDB data set, as they are seen by a Frenet frame observer who moves through all the proteins in our data set. The sphere is centered at the  $C_\alpha$ , and its radius coincides with the length of the (approximately constant) covalent bond. We take the vector  $\mathbf{t}$  that points towards the next  $C_\alpha$  to be in the direction of the positive  $z$ -axis, so that with  $\mathbf{n}$  in the direction of positive  $x$ -axis we have a right-handed Cartesian coordinate system. We introduce the canonical spherical coordinates, so that the angle  $\theta \in [0, \pi]$  measures latitude from the positive  $z$ -axis and the angle  $\varphi \in [0, 2\pi]$  measures longitude in a counterclockwise direction from the  $x$ -axis *i.e.* from the direction of  $\mathbf{n}$  towards that of  $\mathbf{b}$ .

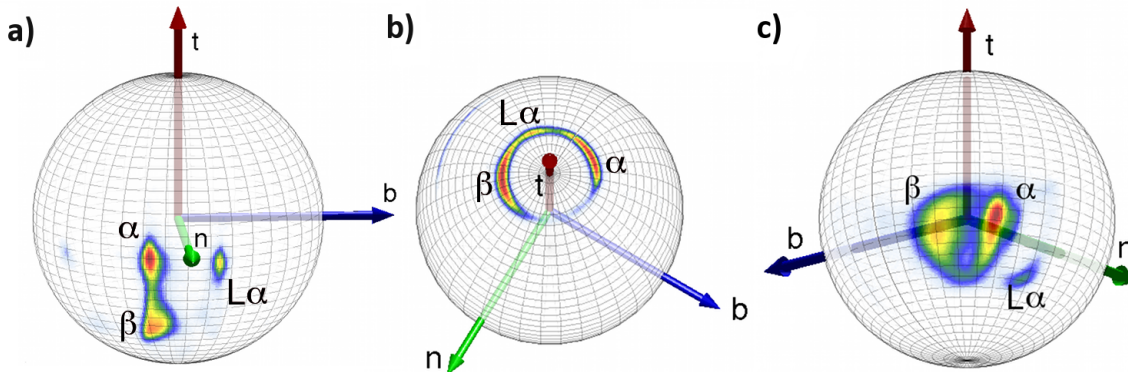


FIG. 1: The locations of a) backbone N-atoms, b) backbone C-atoms c) side-chain  $C_\beta$  atoms, as seen by a Frenet frame observer located at the  $C_\alpha$  carbon at the center of the sphere. In a) the (smaller) point-like direction of backbone N atoms corresponds to the L- $\alpha$  Ramachandran region. The larger region forms a segment of the great circle  $\varphi \approx -15^\circ$ . Note that the loops interpolate latitudinally between  $\alpha$ -helices and  $\beta$ -sheets. In b) the directions of backbone C form a segment of a small circle around  $z$ -axis, with  $\theta \approx 20^\circ$ . The N and C oscillations become coupled into the horse-shoe shaped nutation of  $C_\beta$  as shown in Figure 1c).

We find it remarkable that in the Frenet frame coordinate system, the N and C oscillations shown in Figures 1 (a) and 1 (b) become fully separated into the locally orthogonal  $\theta$  and  $\varphi$  directions respectively; this is not the case in a generic coordinate system. We also find it remarkable that secondary structures such as  $\alpha$ -helices,  $\beta$ -sheets, loops and left-handed  $\alpha$ -regions are all clearly identifiable. Figure 1 (c) then reveals how the N and C oscillations become coupled into a horseshoe shaped nutation of  $C_\beta$ . This nutation is similarly entirely determined by the local secondary structure environment, in an equally systematic manner.

In Figures 2 (a)-(f) we plot the tetrahedral bond angles  $\tau_{NC}$ ,  $\tau_{C\beta}$  and  $\tau_{N\beta}$  separately for the  $\alpha$ -helices, 3/10-helices and  $\beta$ -strands; As in figure 1 the loops will continuously interpolate between these regular secondary structures. The Figures 2 (a) and 2 (d) clearly reveal that the  $\tau_{NC}$  angles depend on the secondary structure in a systematic manner. But we observe no similar effect in either  $\tau_{C\beta}$  or  $\tau_{N\beta}$ . (The isolated small peak in Figure 2 (b) and 2 (e) is due to prolines.)

The fact that *only*  $\tau_{NC}$  in Figure 2 displays systematic secondary structure dependence makes it plain and clear that the paradigm hybridized tetrahedral symmetry of the  $C_\alpha$  carbon atomic orbitals is broken. *In a folded protein the covalent tetrahedral structure around  $C_\alpha$  is not unique.* Instead, the backbone secondary structure breaks the ground state tetrahedral symmetry in a systematic manner which is fully determined by the local secondary structure. We note that for the loop regions, the tetrahedron geometry interpolates deterministically between those of the adjacent regular secondary structures. There is a one-to-one correspondence between the shapes of the  $C_\alpha$  tetrahedra and the way how a protein folds.

On the basis of the present PDB data we are unable to conclude whether the fact that the symmetry breaking is visible only in  $\tau_{NC}$  reflects a true physical effect, or is simply a consequence of the existing refinement procedures that place all the tension on the  $NC$  bond angle. We propose that these details of the symmetry breaking could be investigated in the new generation ultra-high resolution X-ray experiments.

Any molecular dynamics approach [4] to protein folding is based on a harmonic approximation of the energy around the equilibrium values of the bond angles,

$$E_{bond} = \sum_{bonds} K_\theta (\theta - \theta_0)^2 \quad (3)$$

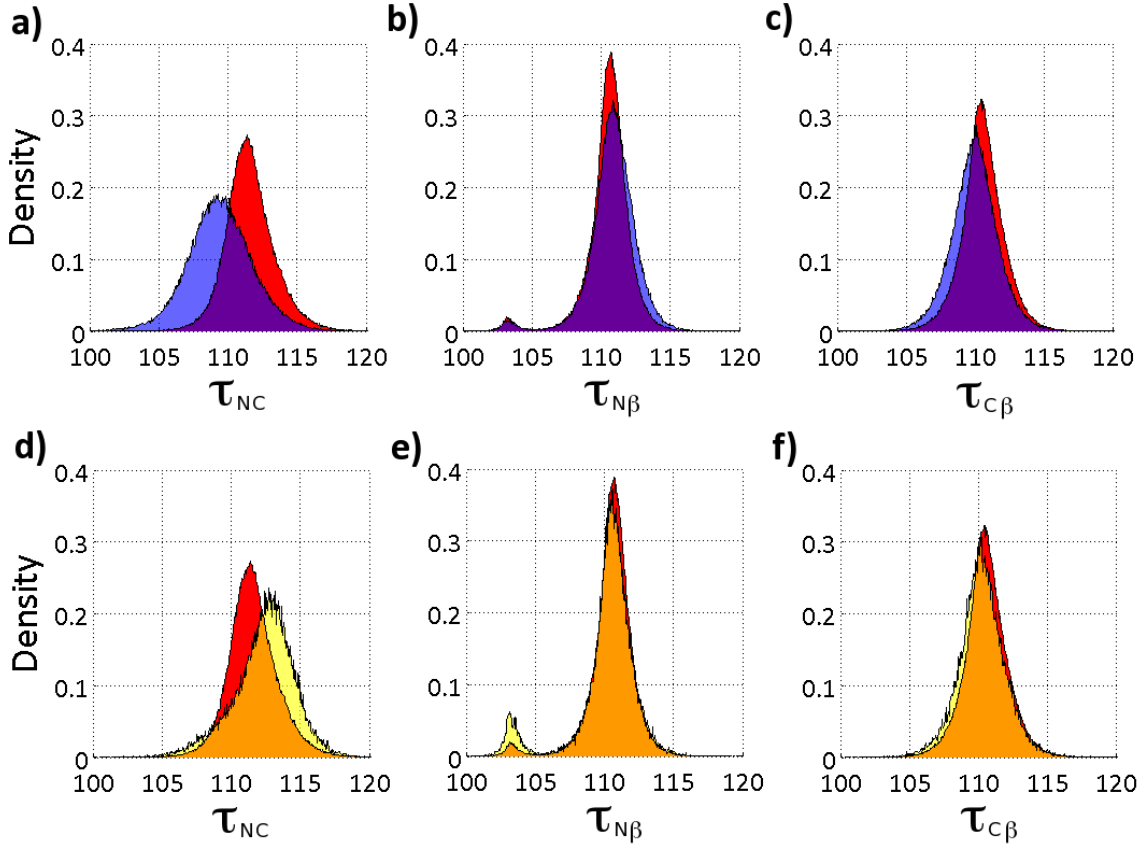


FIG. 2: The probability density angular distribution of the  $\tau_{NC}$ ,  $\tau_{N\beta}$  and  $\tau_{C\beta}$  angles (in degrees) separately for  $\beta$ -strands (blue) and  $\alpha$ -helices (red) in (a)-(c), and separately for 3/10 helices (yellow) and  $\alpha$ -helices (again red) in (d)-(f). The secondary peak in (b) and (e) is proline.

Here the equilibrium values  $\theta_0$  are determined using the paradigm that the  $sp^3$  symmetry of the amino acid remains unbroken and  $\theta_0$  should have *no* dependence on the eventual secondary structure environment. However, Figures 1 and 2 show unequivocally that in actual proteins these equilibrium values depend on the secondary structure in a systematic manner. We now proceed to investigate how to develop an energy function that describes this broken symmetry. Our starting point is the backbone energy function of [12], there it has been shown how the collapsed PDB proteins can be described with experimental B-factor accuracy in terms of soliton solutions to a generalized discrete nonlinear Schrödinger (DNLS) equation. Indeed, the soliton solutions of DNLS equation share a remarkable history with protein research [13], they were first introduced by Davydov to describe the propagation of energy along  $\alpha$ -helices [14]. Mathematically the DNLS equation is *integrable*, there is an infinite hierarchy of conserved quantities [15]. Explicitly the backbone energy function is [12]

$$E = - \sum_{i=1}^{N-1} 2 \kappa_{i+1} \kappa_i + \sum_{i=1}^N \left\{ 2 \kappa_i^2 + q \cdot (\kappa_i^2 - m^2)^2 + \frac{d_\tau}{2} \kappa_i^2 \tau_i^2 - b_\tau \kappa_i^2 \tau_i - a_\tau \tau_i + \frac{c_\tau}{2} \tau_i^2 \right\} \quad (4)$$

Here the first sum together with the three first terms in the second sum comprise the energy function of the conventional DNLS equation, when expressed in the standard Hasimoto variables of fluid mechanics, see [10]- [12] for full details. The fourth ( $b_\tau$ ) and fifth ( $a_\tau$ ) terms are the *only* two lower order nontrivial conserved quantities that appear in the integrable DNLS hierarchy prior to the energy. These are the momentum and the helicity, respectively. The last ( $c_\tau$ ) term is the standard Proca mass term that we add for completeness, it could be ignored with only a minor effect on accuracy. Note in particular that any term odd in the  $\kappa_i$  is excluded by a global  $\mathbb{Z}_2$  symmetry [10]. We also note that the next, higher order conserved quantity in the DNLS hierarchy is the energy function of the modified KdV equation [15]. It could be added, but there is no point since with the present energy function we already reach the experimental B-factor accuracy.

The remarkable property of (4) is that the torsion angle  $\tau_i$  appears at most quadratically so that it can be eliminated

explicitly by using equations of motion. The values of the torsion angle and consequently the entire  $C_\alpha$  backbone geometry becomes then fully determined by bond angle soliton solutions of a generalized DNLS equation [12].

The Figures 1 (a) and (b) reveal that the N and C atoms oscillate independently, in the latitudinal and longitudinal directions respectively. Consequently the ensuing contributions to the protein energy function should also be independent and depend only on the respective angular variables. Together these two independent contributions should then combine into the  $C_\beta$  nutation of Figure 1 (c).

Combining standard universality arguments with the spirit of the harmonic approximation (3), we propose that the latitudinal and longitudinal contributions to protein energy only involve the two lower order conserved quantities in the integrable DNLS hierarchy and the Proca mass. This fixes the ensuing contributions uniquely,

$$E_\theta = \sum_{i=1}^N \left\{ \frac{d_\theta}{2} \kappa_i^2 \theta_i^2 - b_\theta \kappa_i^2 \theta_i - a_\theta \theta_i + \frac{c_\theta}{2} \theta_i^2 \right\} \quad (5)$$

$$E_\varphi = \sum_{i=1}^N \left\{ \frac{d_\varphi}{2} \kappa_i^2 \varphi_i^2 - b_\varphi \kappa_i^2 \varphi_i - a_\varphi \varphi_i + \frac{c_\varphi}{2} \varphi_i^2 \right\} \quad (6)$$

Accordingly the spherical angles  $(\theta_i, \varphi_i)$  are fully determined by the profile of the backbone bond angles  $\kappa_i$  and the *global* parameters that are specific only to a given super-secondary structure. In particular, the tetrahedral symmetry breaking becomes driven by the degenerate ground state structure of the DNLS equation. (We note that the  $\theta_i$  and  $\varphi_i$  variables are coupled to each other only indirectly, by the bond angles  $\kappa_i$ . In particular, the long range interactions that are necessary for describing a collapsed protein are entirely due to the non-local character of the DNLS solitons.)

Since (5), (6) involves both latitudinal and longitudinal angles, the classical solutions of (4)-(6) can be utilized to describe both the backbone  $C_\alpha$  and the side-chain  $C_\beta$  atoms in a folded protein. As an example we inspect the chicken villin headpiece subdomain HP35 with PDB code 1YRF. This is a naturally existing 35-residue protein with three  $\alpha$ -helices separated from each other by two loops. The villin continues to be subject to very extensive studies both experimentally [16]-[18] and *in silico* [19]-[22], and [22] reports on a molecular dynamics construction of folded villin with overall backbone RMSD accuracy around one Ångström. Since the force fields in [19]-[22] utilize the paradigm concept of unbroken  $C_\alpha$  tetrahedral symmetry, the accuracy of in particular [22] can be adopted as a good measure of the symmetry breaking effect.

We first solve for the classical equations of motion for  $\kappa_i$  and  $\tau_i$  from (4), and then construct the remaining angular variables from (5), (6) in terms of  $\kappa_i$ . We use the iterative algorithm and procedure that has been described in [23], [12]. Using the parameters in Table 1 we reach an overall RMSD accuracy 0.39 Å for the combined  $C_\alpha$ - $C_\beta$  configuration which is in line with the experimental B-factor accuracy; see Figure 3 that displays our solution in comparison with the PDB configuration.

Symmetry breaking is a fundamentally important physical phenomenon, often intimately related to structure formation. Here we have shown that a protein backbone breaks the tetrahedral symmetry of the  $sp^3$  hybridized  $C_\alpha$  covalent bonds, in a manner that is entirely determined by the local secondary structure. We have also presented a simple energy function that accounts for the symmetry breaking, to compute the  $C_\beta$  nutation trajectories of the HP35 villin with experimental B-factor accuracy. Our observation is based on the available high precision PDB data, consequently detailed analysis of our symmetry breaking is experimentally feasible. Our observations should have wide applicability in the development of future refinement tools, and for constructing accurate theoretical and computational methods for investigating protein folding dynamics and structure. Indeed, the direct relation between the symmetry breaking and the protein fold geometry suggests that our broken symmetry is intimately connected to the underpinnings of protein folding and thus with the origin of life.

---

\* Electronic address: Martin.Lundgren@physics.uu.se

† Electronic address: Antti.Niemi@physics.uu.se

- [1] I.W. Davis *et.al.*, *Nucl. Acids Res.* **35** 235 (2007)
- [2] R.A. Laskowski *et.al.*, *J. Biomol NMR* **8** 477 (1996)
- [3] X. Qu, R. Swanson, R. Day and J. Tsai, *Curr Protein Pept Sci.* **10** 270 (2009)
- [4] P.L. Freddolino, C.B. Harrison, Y. Liu and Y. Schulten, *Nature Phys.* **6** 751 (2010)
- [5] H.M. Berman *et.al.*, *Nucl. Acids Res.* **28** W375 (2007)
- [6] L. Schäfer and M. Cao, *Journ. Mol. Struc.* **333** 201 (1995)

- [7] P.A. Karplus, Prot. Sci. **5** 1406 (1996)
- [8] D.S. Berkholz, M.V. Shapovalov, R.L. Dunbrack Jr., and P. A. Karplus, Structure **17** 1316 (2009)
- [9] W.G. Touw and G. Vriend, Acta Cryst. **D66** 1341 (2010)
- [10] S. Hu, M. Lundgren, A.J. Niemi, e-print arXiv:1102.5658v1 [q-bio.BM] (Physical Review E, to appear)
- [11] U.H. Danielsson, M. Lundgren, A.J. Niemi, Phys. Rev. **E82** 021910 (2010)
- [12] N. Molkenthin, S. Hu, A.J. Niemi, , Phys. Rev. Lett. **106** 078102 (2011)
- [13] P.G. Kevrekidis, *The Discrete Nonlinear Schrödinger Equation: Mathematical Analysis, Numerical Computations and Physical Perspectives* (Springer-Verlag, Berlin, 2009)
- [14] A.S. Davydov, Journ. Theor. Biol. **66** 379 (1977)
- [15] L.D. Faddeev, L.A. Takhtajan, *Hamiltonian methods in the theory of solitons* (Springer Verlag, Berlin, 1987)
- [16] J. Meng, D. Vardar, Y. Wang, H.C. Guo, J.F. Head and C.J. McKnight, *Biochemistry* **44** 11963 (2005)
- [17] T.K. Chiu, J. Kubelka, R. Herbst-Irmer, W.A. Eaton, J. Hofrichter and D.R. Davies, *Proc. Natl. Acad. Sci. U.S.A* **102** 7517 (2005)
- [18] L. Wickstrom, Y. Bi, V. Hornak, D.P. Raleigh and C. Simmerling, *Biochemistry* **46** 3624 (2007)
- [19] D.L. Ensign, P.M. Kasson and V.S. Pande, *J. Mol. Biol.* **374** 806 (2007)
- [20] H. Lei and Y. Duan, *J. Mol. Biol.* **370** 196 (2007)
- [21] P.L. Freddolino and K. Schulten, *Biophys. Journ.* **97** 2338 (2009)
- [22] D.E. Shaw *et.al.*, Science **330** 341 (2010)
- [23] M. Herrmann, *Appl. Anal.* **89** 1591 (2010)

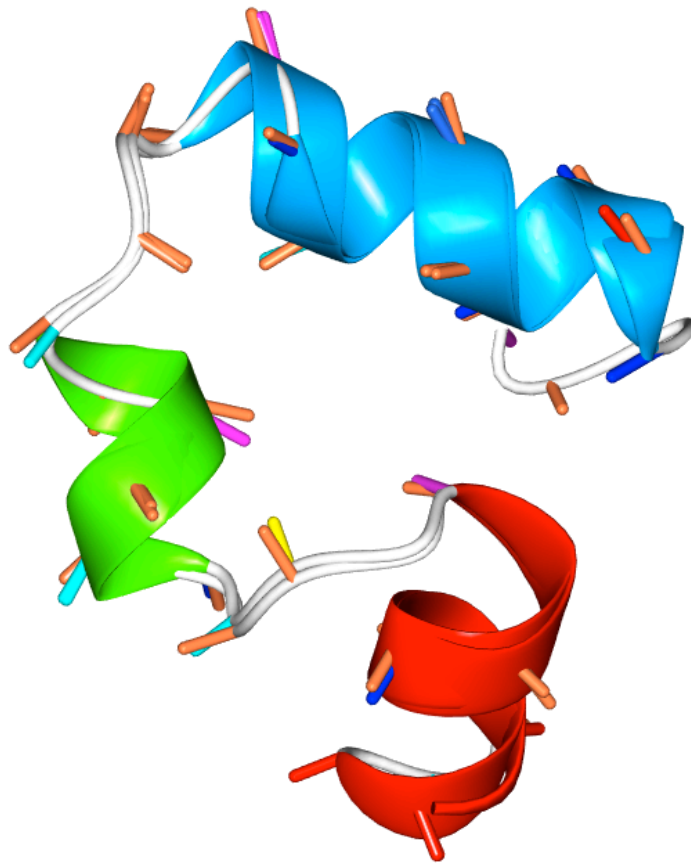


FIG. 3: A cartoon comparison of HP35 with our soliton solution summarized in Table 1. The combined  $C_{\alpha}$  and  $C_{\beta}$  root-mean-square distance is  $0.39 \text{ \AA}$  which is in line with the experimental B-factor accuracy.

parameter	soliton-1	soliton-2
$q_1$	0.459712	0.995867
$q_2$	4.5533320	9.408796
$m_1$	1.504535	1.550322
$m_2$	1.512836	1.535081
$a_\tau$	9.5752137e-9	7.840467e-6
$b_\tau$	-676965e-11	-4.973244e-9
$c_\tau$	4.875744e-9	4.2733696e-6
$d_\tau$	-2.917129e-9	-2.431388e-6
$a_\theta$	1.514770	1.322495
$b_\theta$	-0.0017952	-0.018619
$d_\theta$	0.0420877	6.930946e-8
$a_\varphi$	0.544859	0.3594184
$b_\varphi$	5.66111e-5	3.83253e-4
$d_\varphi$	-0.1845828	-0.226012
RMSD (Å)	0.38	0.32

TABLE I: *Parameter values for the two-soliton solution that describes the two loops of 1YRF with 0.39Å accuracy for both  $C_\alpha$  and  $C_\beta$  atoms. The displayed RMSD values are for the individual solitons. The soliton-1 is located at Glu-45 - Phe-58 and the soliton-2 is located at Phe-58 - Lys-73. We utilize scale invariance to set all  $c_\theta = c_\varphi = 1$ . Notice that the result is sensitive to the accuracy of parameters. This is because a folded protein is a piecewise linear polygonal chain with a positive Liapunov exponent.*